CHEMISTRY
A EUROPEAN JOURNAL

DOI: 10.1002/chem.201001827

High-Temperature Stable, Iron-Based Core–Shell Catalysts for Ammonia Decomposition

Mathias Feyen,[a] Claudia Weidenthaler,[a] Robert Güttel,[a] Klaus Schlichte,[a] Ulrich Holle,[a] An-Hui Lu,*[b] and Ferdi Schüth*[a]

Abstract: High-temperature, stable core–shell catalysts for ammonia decomposition have been synthesized. The highly active catalysts, which were found to be also excellent model systems for fundamental studies, are based on α-Fe_2O_3 nanoparticles coated by porous silica shells. In a bottom-up approach, hematite nanoparticles were firstly obtained from the hydrothermal reaction of ferric chlorides, L-lysine, and water with adjustable average sizes of 35, 47, and 75 nm. Secondly, particles of each size could be coated by a porous silica shell by means of the base-catalyzed hydrolysis of tetraethylorthosilicate (TEOS) with cetyltetramethylammonium bromide (CTABr) as porogen. After calcination, TEM, high-resolution scanning electron microscopy (HR-SEM), energy-dispersive X-ray (EDX), XRD, and nitrogen sorption studies confirmed the successful encapsulation of hematite nanoparticles inside porous silica shells with a thickness of 20 nm, thereby leading to composites with surface areas of approximately 380 $m^2 g^{-1}$ and iron contents between 10.5 and 12.2 wt%. The obtained catalysts were tested in ammonia decomposition. The influence of temperature, iron oxide core size, possible diffusion limitations, and dilution effects of the reagent gas stream with noble gases were studied. The catalysts are highly stable at 750 °C with a space velocity of 120000 $cm^3 g_{cat}^{-1} h^{-1}$ and maintained conversions of around 80% for the testing period time of 33 h. On the basis of the excellent stability under reaction conditions up to 800 °C, the system was investigated by in situ XRD, in which body-centered iron was determined, in addition to FeN_x, as the crystalline phase under reaction conditions above 650 °C.

Keywords: colloids · heterogeneous catalysis · iron · nanotechnology · X-ray diffraction

Introduction

About one-hundred years ago, the discovery of ammonia synthesis by Fritz Haber was a key event that influenced the development of the chemical industry significantly.[1] More recently, the reverse process, decomposition of ammonia into nitrogen and hydrogen, has come into focus as a key step in a possible ammonia-based energy infrastructure.[2] Ammonia plays a major role in this novel infrastructure concept either as hydrogen-storage material or as fuel for direct ammonia fuel cells. For hydrogen production, ammonia decomposition requires temperatures above 400 °C for thermodynamic reasons. Likewise, direct ammonia fuel cells are typically operated at temperatures between 500 and 700 °C. For this reason, highly active catalysts at low temperatures are not urgently required, but the high-temperature stability and long lifetime of the catalysts applied is a more crucial issue.

Core–shell-structured catalysts are a promising approach to solve this problem. They consist of a nanosized catalytic active core that is coated by a porous, thermally stable support. To produce long-term stable materials with fully accessible cores, the shell material has to fulfill several requirements: besides a sufficient mechanical stability and porosity, the shell material should show no mass-transfer resistances and should not negatively affect the catalytic activity of the core under reaction conditions.[3] Based on this concept, several core–shell-structured catalysts have already been devel-

[a] M. Feyen, Dr. C. Weidenthaler, Dr. R. Güttel, K. Schlichte, U. Holle, Prof. Dr. F. Schüth
Department of Heterogeneous Catalysis
Max-Planck-Institut für Kohlenforschung
45470 Mülheim an der Ruhr (Germany)
Fax: (+49) 208-306-2995
E-mail: schueth@mpi-muelheim.mpg.de

[b] Prof. Dr. A.-H. Lu
State Key Laboratory of Fine Chemicals
School of Chemical Engineering
Dalian University of Technology, 116012 Dalian (P.R. China)
Fax: (+86) 411-39608206
E-mail: anhuilu@dlut.edu.cn

Supporting information for this article is available on the WWW under http://dx.doi.org/10.1002/chem.201001827.

oped with noble metals as the core material. Most of the investigated systems consist of Au or Pt nanoparticles in a metal oxide shell, such as silica,[4,5] zirconia,[3] tin oxide,[6] carbon,[7] or cobalt oxide.[8] However, due to the often quite complex multistep preparation pathways, only subgram quantities have been prepared thus far. Therefore, the catalysts are usually used for fundamental studies in CO oxidation, hydrogenation, or reduction reactions. Interestingly, all of these reactions are performed far below 400 °C although the presented shell materials can principally be used for reactions at higher temperatures in which sintering processes play a more crucial role.[6] The catalytic decomposition of ammonia would be a particularly appropriate reaction to exploit the full potential of core–shell-structured catalysts, since the reaction rate increases strongly with increasing temperature. Currently, intensively investigated elements as catalysts for ammonia decomposition are based on ruthenium, iron, nickel, and molybdenum.[9,10] Although ruthenium was found to be the most active catalyst for ammonia decomposition,[11] iron-based catalysts are very attractive materials since the price for the raw material is more than 50000 times lower and more stable, and because the availability of the raw material is higher.[12] To compensate the generally lower activity of iron-based catalysts, higher reaction temperatures can be principally used. However, this approach is usually limited, among other reasons, by enhanced sintering effects of the active phases. As recently shown, hematite nanoparticles protected by a porous silica (pSiO$_2$, in the chosen nomenclature "p" stands for porous) matrix with micro- and mesoporous nature can prevent such sintering effects in ammonia decomposition at temperatures up to approximately 650 °C.[13] However, so far these systems have been only superficially characterized with respect to the stability of their morphology under reaction conditions, their catalytically active phases, or possible mass-transfer limitations caused by the porous silica shell.

Results and Discussion

In this study, we developed a wet chemical route towards high-temperature-stable catalysts based on silica-coated hematite nanoparticles. The schematic pathway is given in Scheme 1. By means of a hydrothermal reaction of ferric chloride in aqueous solution, hematite nanoparticles could be synthesized with three different particle diameters. A defined silica coating of the α-Fe$_2$O$_3$-x (x indicates the rounded α-Fe$_2$O$_3$ particle size) colloids was achieved by using essentially the route developed by Graf et al.[15] By means of polyvinylpyrrolidone (PVP) as surfactant, the α-Fe$_2$O$_3$-x colloids could be coated homogeneously by applying the well-known Stöber process.[16] For the creation of porous SiO$_2$ shells, cetyltrimethylammonium bromide (CTABr) was added to the procedure. After synthesis, the residual organic components were removed by calcination, which led to core–shell composites (α-Fe$_2$O$_3$-x@pSiO$_2$) with accessible iron oxide cores. Under reaction conditions at 800 °C under a pure NH$_3$ stream, the iron oxide cores were reduced to iron and iron nitrides.

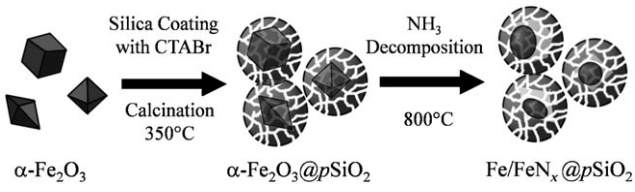

Scheme 1. Schematic pathway for the synthesis and application of high-temperature-stable NH$_3$ decomposition catalysts based on hematite nanoparticles in porous silica shells.

Preparation and characterization of α-Fe$_2$O$_3$-x@pSiO$_2$ core–shell catalysts: As core material, α-Fe$_2$O$_3$ nanoparticles were prepared by the hydrothermal autoclave reaction of L-lysine and ferric chloride at 175 °C in the aqueous phase. By means of this reproducible approach, the size and shape of the resulting colloids could be controlled through the reaction time. For instance, with heating times of 50, 55, and 60 min, average particle sizes of (35±7), (47±9), and (75±19) nm were obtained, as determined from TEM images by taking at least 300 particles into account (Figure 1). The samples were named according to their particle size as α-Fe$_2$O$_3$-35, α-Fe$_2$O$_3$-50, and α-Fe$_2$O$_3$-75. With an increase in diameter, the predominant shape changes from rather spherical particles in α-Fe$_2$O$_3$-35 towards octahedrally shaped particles with sharp edges in α-Fe$_2$O$_3$-75. In α-Fe$_2$O$_3$-50, mainly

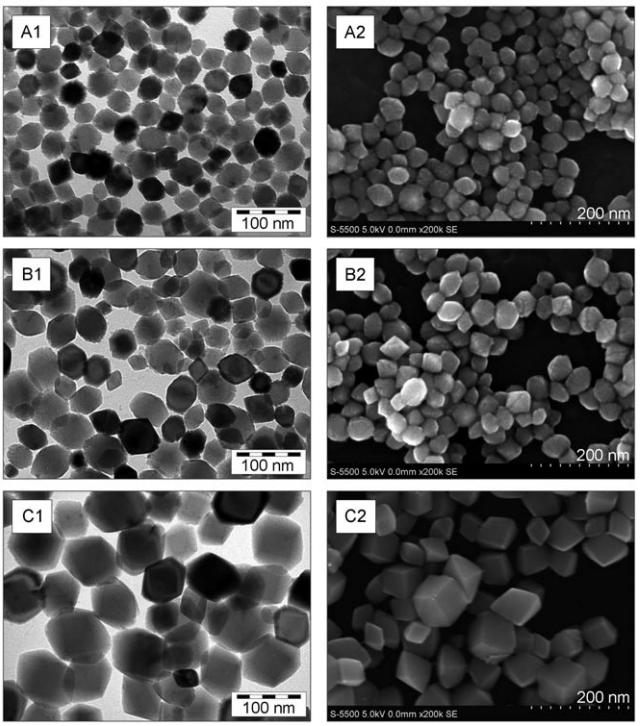

Figure 1. TEM and HR-SEM images of A1), A2) α-Fe$_2$O$_3$-35, B1), B2) α-Fe$_2$O$_3$-50, and C1), C2) α-Fe$_2$O$_3$-75 particles after purification.

intermediate morphologies could be observed. A detailed investigation of the surfaces by means of HR-SEM further reveals a certain roughness of the α-Fe_2O_3-35 particles, which is caused by cracks close to the surface. In comparison, the surface of the octahedrally shaped particles appears smoother. The crystal phases of the three colloids were identified as pure α-Fe_2O_3 by means of XRD (Figure S1 in the Supporting Information). From the line broadening of the reflections, the crystal sizes of α-Fe_2O_3-35, α-Fe_2O_3-50, and α-Fe_2O_3-75 were calculated with the Scherrer equation assuming spherical particles.[17] The resulting diameters of 46, 70, and 78 nm are in reasonable agreement with the TEM analysis.

The encapsulation of the α-Fe_2O_3-*x* with silica was achieved by means of the base-catalyzed hydrolysis of tetraethylorthosilicate (TEOS) in an isopropanol/water mixture. With this so-called Stöber process, the preparation of well-defined core–shell structures is only possible if a homogenous distribution of the colloids could be guaranteed during the whole reaction period.[16] Since the as-prepared hematite colloids would precipitate under the reaction conditions required for the coating, their iron oxide surfaces needed to be modified with polyvinylpyrrolidone (PVP) K90 before this step. In addition, the cationic surfactant cetyltetramethylammonium bromide (CTABr) was added during the silica-coating step to induce porosity of the silica shells in the final product. After reaction, the obtained α-Fe_2O_3-*x*@*p*SiO_2 composites were purified by centrifugation and subsequently calcined at 350 °C. TEM and XRD investigations confirmed the complete coating of the α-Fe_2O_3-*x* cores, which were otherwise unchanged, with an average silica shell thickness of 20 nm (Figure 2, Figure 3A and B, and Figure S2 in the Supporting Information). Besides the target core–shell structures, no separate iron oxide particles or incomplete silica shells could be found in the sample.

To visualize the porous surfaces of the silica, HR-SEM images were used. Two representative images of α-Fe_2O_3-50@*p*SiO_2 in different magnifications are shown in Figure 2C and D. Judging from the HR-SEM and TEM images, the pores of the materials appear to be smaller than 2 nm but they are clearly visible. To confirm the porous nature of the silica shells, nitrogen sorption measurements were performed to estimate the pore parameters. The corresponding isotherms are presented in Figure 4. The Brunauer–

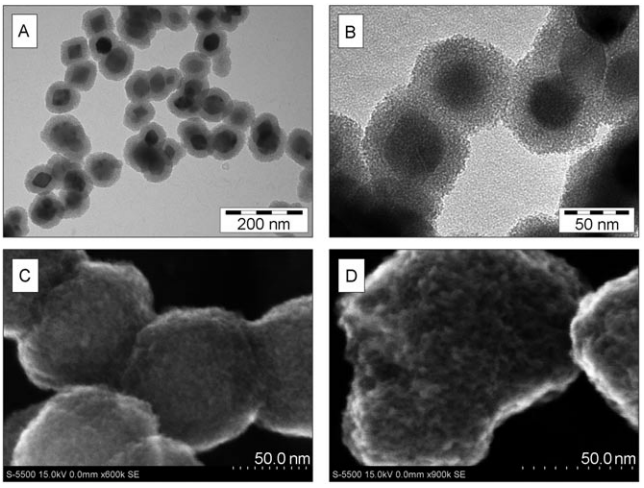

Figure 2. A), B) TEM and C), D) HR-SEM images of α-Fe_2O_3-50@*p*SiO_2 in two different magnifications, respectively.

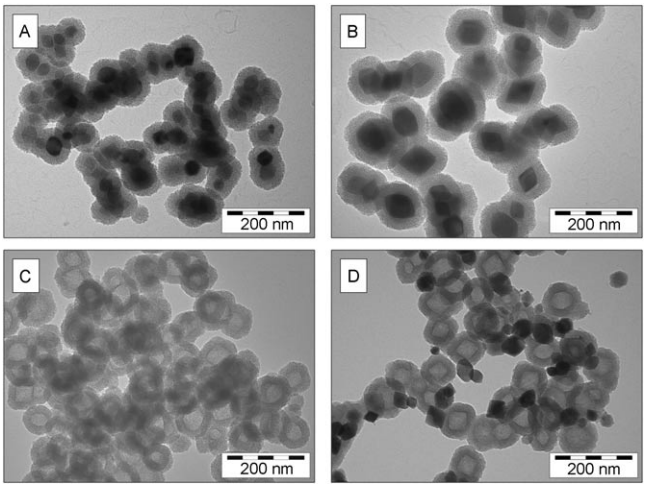

Figure 3. TEM images of A) α-Fe_2O_3-35@*p*SiO_2, B) α-Fe_2O_3-75@*p*SiO_2, C) @*p*SiO_2, and D) α-Fe_2O_3-50 + @*p*SiO_2 after calcination, respectively.

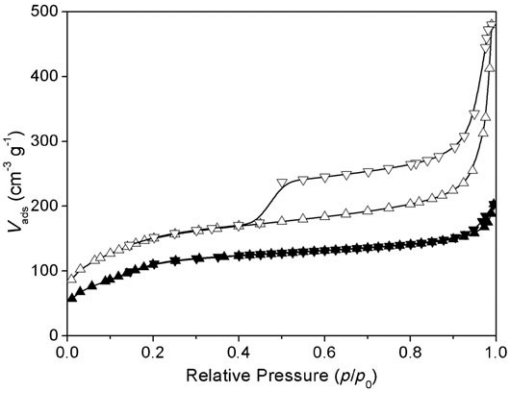

Figure 4. Nitrogen sorption results for α-Fe_2O_3-50@*p*SiO_2 (▲: adsorption, ▼: desorption) and for @*p*SiO_2 (△: adsorption, ▽: desorption) after calcination.

Emmett–Teller (BET) surface area and the micropore volume of the composite are 382 $m^2 g^{-1}$ and 0.15 $cm^3 g^{-1}$, respectively. Indeed, these values are too high for dense spherical silica particles in this size range, thereby confirming the porous nature of the silica shells.

The elemental composition of the Fe_2O_3-*x*@*p*SiO_2 catalysts was analyzed by energy-dispersive X-ray (EDX) mapping. In Table 1, the obtained values for Fe, Si, and O are summarized. The results show comparable contents of Fe_2O_3 (calculated from the results for Fe) with 38.0 wt% in α-Fe_2O_3-35@*p*SiO_2, 42.0 wt% in α-Fe_2O_3-50@*p*SiO_2, and

Table 1. Elemental composition of the prepared catalysts obtained from EDX.

Sample	Fe atom [%]	Si atom [%]	O atom [%]
α-Fe_2O_3-35@*p*SiO_2	10.5	21.6	67.0
α-Fe_2O_3-50@*p*SiO_2	12.2	19.5	68.3
α-Fe_2O_3-75@*p*SiO_2	10.5	18.1	71.3
α-Fe_2O_3-50+@*p*SiO_2	7.5	23.0	69.9

37.5 wt% in α-Fe_2O_3-75@*p*SiO_2. Besides the hematite phase, Si and O were found in the atomic ratios of approximately 1:2.5. With the exception of traces of carbon, no other elements were detected in the samples by using this method. In our experiments, the process could be scaled up by a factor of four. Hence, from one single batch more than one gram of core–shell-structured catalyst could be obtained without any decrease in product quality.

As a reference material (labeled as α-Fe_2O_3-50+@*p*SiO_2), α-Fe_2O_3-50 nanoparticles were deposited on porous hollow silica spheres obtained from acid-leached α-Fe_2O_3-50@*p*SiO_2 catalysts. The aim was the preparation of material with a comparable composition of α-Fe_2O_3 nanoparticles and porous SiO_2 shells like in α-Fe_2O_3-50@*p*SiO_2, but with a different morphology. The porous hollow silica spheres were investigated by TEM and nitrogen sorption to confirm the complete removal of the iron oxide cores (Figure 3C and Figure 4).

The N_2-sorption measurements of the leached, washed, and calcined hollow @*p*SiO_2 particles showed a BET surface area of 522.7 $m^2 g^{-1}$ and a micropore volume of 0.18 $cm^3 g^{-1}$. In comparison with α-Fe_2O_3-50@*p*SiO_2, the higher surface area and micropore volume are explicable by the lower material density and the accessible internal pore inside the hollow silica spheres. The step in the desorption branch of the @*p*SiO_2 material at $p/p_0 \approx 0.45$ relates to the internal void, which appears after the removal of the α-Fe_2O_3 cores. The nitrogen from the internal void is released suddenly through the narrow pores in the shells when the meniscus becomes unstable at a relative pressure (p/p_0) of approximately 0.45. After drying, the obtained @*p*SiO_2 support was mixed with a dispersion of α-Fe_2O_3-50 nanoparticles, which could be deposited on the silica supports by drying and calcination. As can be seen in Figure 3D, the iron oxide nanoparticles were found randomly assembled on the surface of the porous SiO_2 hollow spheres. EDX analysis revealed a Fe_2O_3 content of 27.4 wt% beside silica and oxygen, which were present in the ratio of around 1:2.5.

Catalytic performance of α-Fe_2O_3-*x*@*p*SiO_2 core–shell catalysts: The prepared materials were analyzed in the ammonia decomposition reaction with respect to their core-size-dependent activities, high-temperature stability, and phase transformation behavior. Prior to catalysis, all composites were treated at 550°C under hydrogen for activation. For the example of α-Fe_2O_3-50@*p*SiO_2 (Figure S2 in the Supporting Information), it was shown by ex situ XRD that the α-Fe_2O_3 cores were reduced to 30 nm-sized α-Fe crystals with Fe_3O_4 as a side phase. The catalytic activity of the materials was tested in four runs with a space velocity of 15000 $cm^3 g_{cat}^{-1} h^{-1}$ of pure NH_3. The first two runs were performed from 350 up to 700°C, whereas during the last two runs the catalyst was heated from 350 to 800°C to study the temperature stability. The observed conversion–temperature curves of the four runs with α-Fe_2O_3-50@*p*SiO_2 plotted in Figure 5 are representative of all three α-Fe_2O_3-*x*@*p*SiO_2 materials.

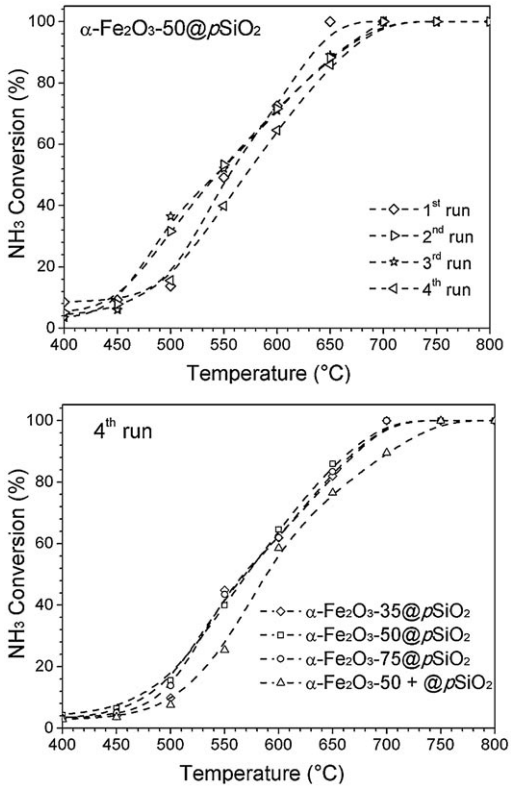

Figure 5. Conversion–temperature curves. Top: cycle stability for α-Fe_2O_3-50@*p*SiO_2 as an example. Bottom: comparison of the fourth run for different materials. NH_3 flow rate of 15000 $cm^3 g_{cat}^{-1} h^{-1}$.

Starting from 10% conversion at 400°C in the first run, the decomposition rate of ammonia increases approximately linearly between 500 to 650°C, at which full conversion of NH_3 was reached. On the basis of this data, it can be assumed that the iron-based cores are still accessible for the reagent species. The conversion–temperature curves in the next three runs were basically identical within the error limits. Full conversion was reached in all cases at 700°C. With respect to a reasonable analytical error, the catalyst shows no deactivation up to 800°C during the reaction tests.

Similar catalytic activities were found for the other catalysts in the first three runs, although different core sizes with originally different shapes were used. Under these conditions, the average activity is comparable with other, related iron-based catalyst systems.[13] Figure 5 compares the conversions over all materials during the fourth catalytic run. α-

Fe_2O_3-50+@$p$$SiO_2$ showed slightly lower conversions in comparison to the α-Fe_2O_3-x@$p$$SiO_2$ composites. With this reference material, full NH_3 conversion was not reached before 750 °C; this could be an indication of a more pronounced deactivation, which was confirmed in subsequent experiments (see below). To check whether the morphology of this catalyst also changes, the used catalysts were analyzed by TEM. The results are shown in Figure 6 and con-

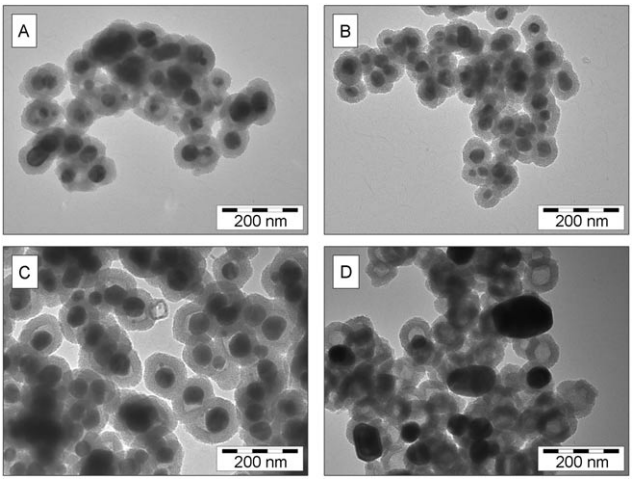

Figure 6. TEM images of A) α-Fe_2O_3-35@$p$$SiO_2$, B) α-$Fe_2O_3$-50@$p$$SiO_2$, C) α-$Fe_2O_3$-75@$p$$SiO_2$, and D) α-$Fe_2O_3$-50+@$p$$SiO_2$ after four catalytic runs with temperatures up to 800 °C.

firm the good temperature stability of the prepared core–shell systems. No visible agglomeration effects occurred in the core–shell catalysts during the catalytic tests up to 800 °C. All iron-based particles were still centered within the unchanged porous SiO_2 shells. The core size (between 35 and 75 nm) obviously does not have a significant effect on the catalytic performance of the catalysts, since the amounts of iron are comparable. In contrast, the iron particles in α-Fe_2O_3-50+@$p$$SiO_2$ formed irregularly shaped particles with sizes up to 150 nm due to agglomeration, whereas the hollow SiO_2 support remained unchanged.

Ex situ XRD analysis of the catalysts after cooling down revealed the formation of ε-phase Fe_3N/Fe_2N and Fe_4N, with traces of hematite as a side phase, which is in agreement with the literature (Figure S4a in the Supporting Information).[18] For this reason, the observed volume shrinkage of the iron-based cores in the core–shell catalysts can be attributed to reduction processes during hydrogen treatment and/or during reaction. The differentiation between ε-Fe_3N and ε-Fe_2N from powder diffraction data is very complicated. Both phases consist of a hexagonal close-packed arrangement of iron atoms with nearly the same unit-cell parameters. Different ordering of nitrogen on the interstitial positions leads to the formation of superstructures.[19–21] Whereas only one-third of the octahedral interstices in the ε-Fe_3N structure is occupied by nitrogen atoms, one-half is occupied in the ε-Fe_2N structure. The higher nitrogen content is realized by the occupancy of an additional nitrogen position, which results in the appearance of additional weak reflections in the powder pattern of ε-Fe_2N. Since neither the presence nor the absence of these additional reflections can be confirmed by our data, the phase will be denoted in the following as ε-$Fe_{3-x}N$ (with $0 \leq x \geq 1$).

To further demonstrate the high-temperature stability of the core–shell-structured catalysts, a long-duration stability test was performed with α-Fe_2O_3-50@$p$$SiO_2$ and α-Fe_2O_3-50+@$p$$SiO_2$. For the test, the catalysts were reduced under hydrogen according to the description given above and heated up to 750 °C under an ammonia flow rate of 120000 $cm^3 g_{cat}^{-1} h^{-1}$. At the beginning, 80 % conversion was reached for both catalyst systems (Figure 7). This indicates

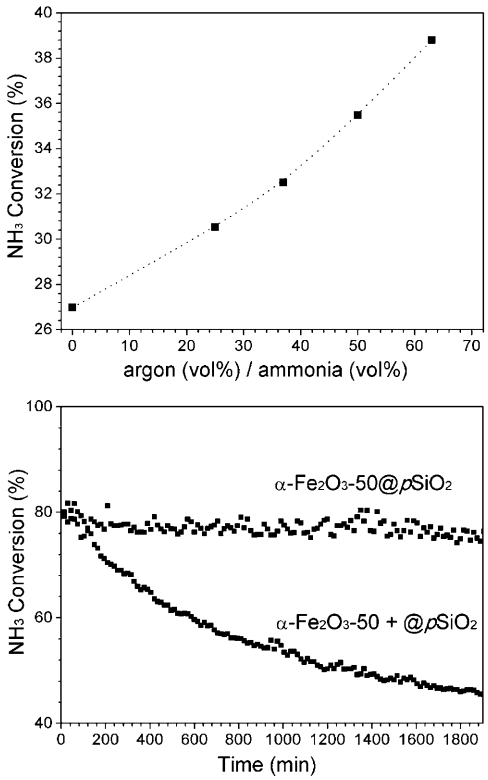

Figure 7. Top: stability test of α-Fe_2O_3-50@$p$$SiO_2$ and α-Fe_2O_3-50+@$p$$SiO_2$ in NH_3 decomposition reaction at 750 °C with an NH_3 flow rate of 120000 $cm^3 g_{cat}^{-1} h^{-1}$. Bottom: dependency of the NH_3 conversion on the dilution of the reagent stream with argon at 600 °C; NH_3 flow rate of 30000 $cm^3 g_{cat}^{-1} h^{-1}$.

the absence of mass-transfer limitations for α-Fe_2O_3-x@$p$$SiO_2$ through the porous SiO_2 shell at these relatively high temperatures. Over the 33 h reaction time, the conversion of α-Fe_2O_3-50@$p$$SiO_2$ stayed almost constant with a conversion of 78 % at the end. In contrast, the reference material α-Fe_2O_3-50+@$p$$SiO_2$ deactivated right from the beginning, thus resulting in conversions of less than 45 % after 33 h. TEM images of the used catalyst are again in agreement with the catalytic data (Figure S4 in the Supporting Information). Whereas the core–shell catalyst showed no

change in morphology and size, the iron species in α-Fe_2O_3-50+@*p*SiO_2 sintered to large particle clusters, which were identified by means of ex situ XRD as ε-$Fe_{3-x}N$. Therefore, the agglomeration effects and/or the formation of another crystalline phase under these reaction conditions can be the reason for the deactivation of the reference catalyst.

Based on the high stability of the prepared core–shell catalysts, further studies could be performed to gain a deeper insight into the activity-dependent parameters of the decomposition reaction. Therefore, an NH_3 gas stream was diluted with the noble gas argon. The dilution of the educt stream provides a faster removal of the product gases from the catalyst, which could influence the reaction equilibrium. For the catalytic test, Fe_2O_3-50@*p*SiO_2 was reduced as described above under hydrogen and heated to 600 °C. At an NH_3 flow rate of 30000 $cm^3 g_{cat}^{-1} h^{-1}$, the catalyst was equilibrated for 24 h. Afterwards, the constant NH_3 flow was stepwise diluted by argon up to 63 mol % Ar, whereas all other parameters (including the NH_3 flow) were kept constant. The detected NH_3 conversion was plotted as a function of the molar fraction of argon in the inlet gas stream (Figure 7). Clearly, the conversion increases in the analyzed range from 27 to 39 %.

To interpret this data set, mainly two effects—caused by the dilution with argon—have to be taken into account. From the literature it is known that especially the reaction order of hydrogen can be negative depending on the type of catalyst.[22,23] Therefore, a dilution of the product gases should increase the overall reaction rate of the catalyst. The opposite could be expected for dilution of the reagent: if the ammonia concentration enters with a positive reaction order in the kinetics, a dilution with noble gases would lead to a reduction of the reaction rate. Since the conversion increases with the dilution of the reactive gases in our experiments, it can be assumed that the overall conversion of this system is governed by hydrogen concentration in the reactor. A formation of iron silicates due to the change of the inlet gas mixture could be excluded by means of ex situ XRD measurements.

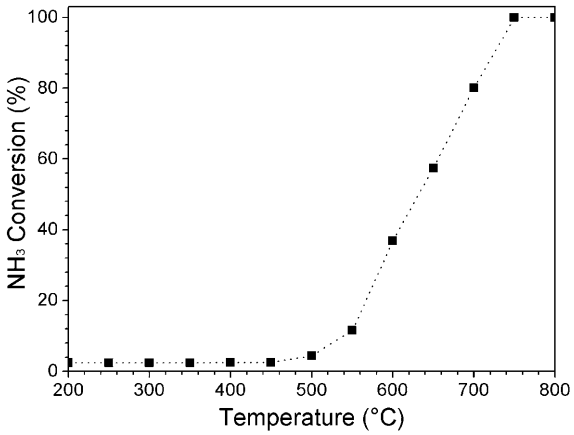

Figure 8. Conversion–temperature curve of the first run for α-Fe_2O_3-50@*p*SiO_2 at a flow rate of 120000 $cm^3 g_{cat}^{-1} h^{-1}$.

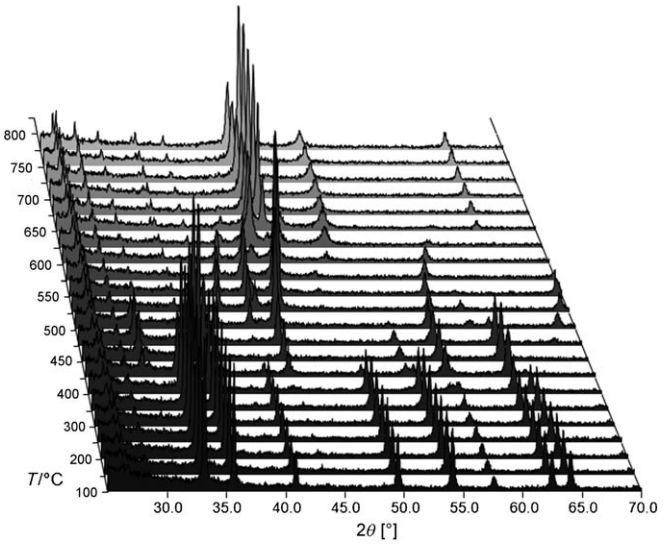

Figure 9. X-ray diffraction patterns collected in situ during ammonia decomposition in the temperature range between 100 and 775 °C with $Cu_{K\alpha 1,2}$ radiation. A detailed description of phase-formation processes is given in the text.

In situ XRD studies on α-Fe_2O_3-*x*@*p*SiO_2 core–shell catalysts: To obtain more information about the phase transformations that occur during the NH_3 decomposition reaction, in situ X-ray diffraction experiments were performed (Figure 9) on the as-prepared α-Fe_2O_3-75@*p*SiO_2 catalysts. The diffraction patterns were recorded under simulated reaction conditions to allow a direct assignment of the crystalline phases with conversion data (observed in the quartz tube reactor) at different temperatures (Figure 8). For the in situ analysis of the phase composition by XRD, a space velocity of 120000 $cm^3 g^{-1} h^{-1}$ was selected to work under comparable conditions as those during the activity test. In our studies, the first catalytic run of the as-prepared α-Fe_2O_3-75@*p*SiO_2 catalyst was analyzed by each analysis method in the temperature range between 200 and 800 °C. In the in situ XRD tests as well as in the quartz-tube-reactor experiments, the catalysts were equilibrated for at least 30 min at each measurement temperature. Up to 350 °C, the as-prepared catalyst consists of pure α-Fe_2O_3 as a crystalline phase and the conversion of ammonia stayed below 3 %. Between 400 and 450 °C, the hematite phase was reduced to magnetite (Fe_3O_4) with hematite as the side phase. At 500 °C, new reflections appear simultaneously with a slight increase in the ammonia conversion to 5 %, whereas the magnetite reflections start to disappear. They match ε-$Fe_{3-x}N$, which shows increasing disorder of the nitrogen atoms as temperature increases.[21]

A further increase of temperature to 525 °C leads to a proceeding reduction of iron, and FeO is formed as a crystalline phase together with Fe_3N_{1+x}. At 550 °C, the amount of FeO is very low, and the nitride reflections are significantly shifted to higher diffraction angles. This shift is

caused by a decrease of the lattice parameters with increasing temperature, thereby indicating a change in the chemical composition. At this temperature, an ammonia conversion of 11% was determined. Following the heating ramp, Fe_4N was additionally formed at 575°C. A significant change of the powder pattern is observed at 625°C. FeN_x was formed in addition to an unidentified phase. The compound could not be assigned to any known FeN phase, although the conversion increases significantly to 48%. At 650°C, iron had been formed (body-centered structure) and was accompanied by an increase in conversion of 9%. Full conversion was reached at 750°C with FeN_x and Fe as stable crystalline phases up to 775°C. Therefore, it can be stated that iron is the prevailing phase in the ammonia decomposition at temperatures above 650°C, which is in line with recent literature reports.[23,24] Keeping the sample under the reaction conditions for several hours does not change the phase composition or the crystallite sizes.

Depending on the cooling rate during the following cooling process, different crystalline phases could be obtained in the used catalysts that deviate from those under reaction conditions. If the catalyst was cooled at 1.5°C min^{-1} from 800°C to room temperature (under an ammonia atmosphere), only ε-$Fe_{3-x}N$ and Fe_4N were found in the final composite (Figure 10). This experiment shows that slow cooling

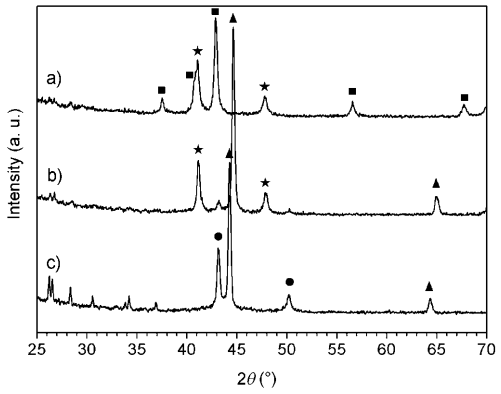

Figure 10. Powder patterns for FeN_x (●), Fe (▲), Fe_4N (★), and ε-$Fe_{3-x}N$ (■) collected in situ under ammonia atmosphere at a) 800°C, b) after rapid cooling (≈20°C min^{-1}) to room temperature, and c) after slow cooling (≈1.5°C min^{-1}) to room temperature with $Cu_{K\alpha1,2}$ radiation. Both cooling experiments were performed under an ammonia atmosphere. The additional reflections between $2\theta = 25$ and 37° are caused by the sample holder.

under an ammonia atmosphere leads to a reaction of iron with nitrogen and the formation of iron nitrides during the cooling process. In contrast, if the catalysts were quickly cooled down under similar conditions, FeN_x transformed to Fe_4N (roaldite) and small amounts of ε-$Fe_{3-x}N$, whereas iron remained present as a crystalline phase. The studies reveal that the phase composition of the catalyst analyzed under reaction conditions in situ may not be comparable with that determined in ex situ experiments at room temperature. Further, the experiments reveal the presence of body-centered iron under the given reaction conditions above 650°C.

Conclusion

In summary, we have demonstrated the successful preparation of core–shell-nanostructured ammonia decomposition catalysts with iron/iron nitride cores as the active component. The catalysts show, particularly at temperatures above 600°C, high reaction rates while maintaining stability up to 800°C. For instance, 73 kg $NH_3\,kg_{cat}^{-1}\,h^{-1}$ could be decomposed at a reaction temperature of 750°C. No diffusion limitations, which could have been caused by the porous silica shells, could be detected up to flow rates of 120000 $cm^3\,g_{cat}^{-1}\,h^{-1}$. In addition, we observed that the particle size seems to have only a limited influence on the catalytic activity in the diameter range between 35 and 75 nm. The inferior stability and long-term activity of core–shell-structured catalysts could be demonstrated by means of a reference material that consisted of similar components but without a core–shell structure. For the first time, the crystalline phases were analyzed by in situ XRD under reaction conditions that reveal the presence of body-centered iron and FeN_x under reaction conditions above 650°C. Body-centered iron and FeN_x are supposed to be the most active iron phases for ammonia decomposition. Furthermore, it was observed that the cooling rate after reaction has a strong influence on the finally observed iron and iron nitride phases.

Experimental Section

Chemicals: Ammonium hydroxide solution (28 wt%) in water was purchased from Fluka. Iron(III)chloride hexahydrate (≥99%), L-lysine (>99.0%), cetyltrimethylammonium bromide (CTABr, 98%), polyvinylpyrrolidone K90 (PVP-90), and tetraethylorthosilicate (TEOS) (98.0%) were purchased from Sigma Aldrich. Hydrochloric acid (37% in water) was received from J.T. Baker. Furthermore, isopropanol and ethanol were used in technical-grade quality.

Preparation of α-Fe_2O_3 nanoparticles: α-Fe_2O_3 nanoparticles were synthesized according to a modified route that was previously reported.[14] Briefly, $FeCl_3{\cdot}6H_2O$ (2 mmol) and L-lysine (2 mmol) were dissolved in Millipore water (100 mL, 18.2 MΩ cm^{-1}). The solution was heated up to 175°C in a steel autoclave with a Teflon inlet that has an inner volume of 110 cm^3. The size of the α-Fe_2O_3-*x* crystals was controlled by the heating time and is indicated by the value of *x* in the sample nomenclature. The individual reaction parameters are listed in Table 2. After reaction, the resultant colloids were centrifuged for the given times with the listed relative centrifugal force (RCF) values and washed three times with water to remove residues of unreacted iron species and organic compounds. In

Table 2. Synthesis parameters for the preparation of α-Fe_2O_3-*x* colloids (*x* indicates the rounded α-Fe_2O_3 particle size).

Sample	Heating time [min]	RCF [g]	Centrifugation time [min]	d_{TEM} [nm]	Standard deviation [nm]
α-Fe_2O_3-35	50	29200	15	35	±7
α-Fe_2O_3-50	55	21000	12	47	±9
α-Fe_2O_3-75	60	15500	10	72	±19

between washing and centrifugation, the colloids were redispersed by ultrasonication in the aqueous phase.

Encapsulation of α-Fe_2O_3-*x* nanoparticles in porous SiO_2 spheres: To achieve a homogeneous distribution of the prepared α-Fe_2O_3-*x* nanoparticles during the Stöber process, an addition of PVP-K90 is required. Therefore, α-Fe_2O_3-*x* nanoparticles (100 mg) were stirred with a solution of PVP-K90 (300 mg) in H_2O (50 mL) for 24 h at 25 °C. For the encapsulation of α-Fe_2O_3-*x* nanoparticles in porous SiO_2 shells, CTABr was used as a porogen. In the synthesis, PVP-K90-stabilized α-Fe_2O_3-*x* nanoparticles (100 mg) in H_2O (50 mL) were stirred together with CTABr (300 mg) in isopropanol (200 mL). After 1 h, isopropanol (200 mL) and concentrated ammonia solution (4 mL, 28 % NH_3 in H_2O) were added and stirred again with the colloids for 1 h. To start the hydrolysis reaction, TEOS (600 μL) was given in one shot to the stirred dispersion. After 20 h reaction time, the solids were purified in ethanol by centrifugation as described above (see the section that describes the preparation of α-Fe_2O_3 nanoparticles). The dried powder was finally calcined at 350 °C for 1 h to remove organic compounds from the porous SiO_2 shells. Through this approach, about 260 mg of core–shell particles could be obtained from 100 mg α-Fe_2O_3-*x*. The obtained red solids were now ready for use as catalysts in ammonia decomposition.

Preparation of hollow @SiO_2 spheres for the preparation of α-Fe_2O_3-50 + @*p*SiO_2: To remove the iron oxide cores from the α-Fe_2O_3-50@*p*SiO_2 composites, typically colloids (40 mg) were stirred at 25 °C in concentrated hydrochloric acid (9 mL, 37 % HCl in H_2O) for 12 h. Afterwards, the residual solid material was purified by centrifugation and washing with water as described in the section on the preparation of α-Fe_2O_3 nanoparticles. After drying, the white solid (20 mg) was mixed with α-Fe_2O_3-50 (7.0 mg) dispersed in H_2O (2 mL). Finally, the material was dried at 90 °C and calcined at 350 °C for 1 h under air.

Characterization: For ex situ experiments, the X-ray powder patterns were recorded using a Stoe STADI P transmission diffractometer in Debye–Scherrer geometry ($Mo_{K\alpha1}$, $\lambda = 0.70930$ Å) with a primary monochromator and a position-sensitive detector. The in situ experiments were performed using a reaction chamber (Anton Paar XRK900) mounted on a Bragg Brentano diffractometer (PANalytical, X'Pert Pro, $Cu_{K\alpha}$: $\lambda = 1.54056$ Å). The sample (46 mg) was prepared in a MARCOR sample holder (10 mm diameter, 1.5 mm depth) and heated up from room temperature to 800 °C in a dry NH_3 atmosphere with a heating rate of 20 °C min^{-1}. The reaction gas flowed through the sample with a flow rate set to 15000 $cm^3 g^{-1} h^{-1}$. After the measurements, the catalyst was cooled down from 800 °C to room temperature with cooling rates of 20 or 1.5 °C min^{-1}. TEM and STEM analyses were carried out using a Hitachi HF 7500 and a Hitachi S-5500 microscope, respectively. All samples were prepared on carbon film supported by a copper grid. N_2 sorption measurements were performed using a Micrometrics ASAP 2010 instrument. Prior to analysis, the samples were activated under vacuum for 10 h at 200 °C. X-ray (EDX) analyses were performed using a Hitachi S-3500 N instrument equipped with an Oxford EDX unit (INCA Surveyor Imaging System).

Catalytic reaction: For the ammonia decomposition reaction, the dried α-Fe_2O_3-*x*@*p*SiO_2 catalyst (25 mg) was loaded on a frit in a quartz-tube, fixed-bed reactor with an internal diameter of 6 mm. The materials were activated under hydrogen flow (15000 $cm^3 g_{cat}^{-1} h^{-1}$) at 550 °C for 1 h. Subsequently, the temperature was decreased to 350 °C and the gas flow was switched to pure NH_3. Depending on the measurement, the NH_3 flow was varied between 7500 and 120000 $cm^3 g_{cat}^{-1} h^{-1}$. The specific flow rate for each experiment is given in the corresponding results section. For temperature-dependent conversion measurements of NH_3, the temperature was varied between 350 and 800 °C in 50° steps. For each temperature, four values were recorded within 30 min under steady-state conditions using a micro-GC (Agilent). The GC is equipped with a thermal conductivity detector (TCD) to detect NH_3 in a carrier gas flow of He. Typically, four catalytic runs were conducted. The catalyst bed was heated from 350 °C to the desired temperature for the investigation of activation effects, catalyst stability, and recyclability. In between the catalytic runs, the samples were cooled down again to 350 °C under NH_3 flow. After catalysis, the catalysts were cooled from 800 °C down to room temperature with a rate of approximately 10 °C min^{-1} under ammonia flow.

Acknowledgements

The authors thank Mr. Bongard for the measurement of the HR-SEM images.

[1] F. Haber, Kaiserliches Patentamt DE235421, **1911**.
[2] S. F. Yin, B. Q. Xu, X. P. Zhou, C. T. Au, *Appl. Catal. A* **2004**, *277*, 1–9.
[3] P. M. Arnal, M. Comotti, F. Schüth, *Angew. Chem.* **2006**, *118*, 8404–8407; *Angew. Chem. Int. Ed.* **2006**, *45*, 8224–8227.
[4] J. Lee, J. C. Park, H. Song, *Adv. Mater.* **2008**, *20*, 1523–1528.
[5] S. H. Joo, J. Y. Park, C.-K. Tsung, Y. Yamada, G. A. Somorjai, *Nat. Mater.* **2009**, *8*, 126–131.
[6] K. Yu, Z. C. Wu, R. Q. Zhao, B. X. Li, Y. Xie, *J. Phys. Chem. C* **2008**, *112*, 2244–2247.
[7] S. Ikeda, S. Ishino, T. Haranda, N. Okamoto, T. Sakata, H. Mori, S. Kuwabata, T. Torimoto, M. Matsumura, *Angew. Chem.* **2006**, *118*, 7221–7224; *Angew. Chem. Int. Ed.* **2006**, *45*, 7063–7066.
[8] Y. Yin, R. M. Rioux, C. K. Erdonmez, S. Hughes, G. A. Somorjai, A. P. Alivisatos, *Science* **2004**, *304*, 711–714.
[9] P. M. Arnal, C. Weidenthaler, F. Schüth, *Chem. Mater.* **2006**, *18*, 2733–2739.
[10] J. C. Ganley, F. S. Thomas, E. G. Seebauer, R. I. Masel, *Catal. Lett.* **2004**, *96*, 117–122.
[11] W. Raróg-Pilecka, D. Szmigiel, Z. Kowalczyk, S. Jodzis, J. Zielinski, *J. Catal.* **2004**, *221–228*, 465–471.
[12] E. van Steen, M. Claeys, *Chem. Eng. Technol.* **2008**, *31*, 655–666.
[13] Y. Li, S. Liu, L. Yao, W. Ji, C.-T. Au, *Catal. Commun.* **2010**, *11*, 368–372.
[14] G.-H. Wang, W.-C. Li, K.-M. Jia, B. Spliethoff, F. Schüth, A.-H. Lu, *Appl. Catal. A* **2009**, *364*, 42–47.
[15] C. Graf, S. Dembski, A. Hofmann, E. Rühl, *Langmuir* **2006**, *22*, 5604–5610.
[16] W. Stöber, A. Fink, E. Bohn, *J. Colloid Interface Sci.* **1968**, *26*, 62–69.
[17] P. Scherrer, *Nachr. Ges. Wiss. Goettingen Math.-Phys. Kl. Fachgruppe 2* **1918**, 98.
[18] R. Schlögl, G. Ertl, H. Knözinger, F. Schüth, J. Weitkamp in *Handbook of Heterogeneous Catalysis* (Eds.: R. Schlögl), Wiley-VCH, Weinheim, **2008**, pp. 2509–2575.
[19] Z. Q. Liu, D. X. Li. , Z. K. Hei, H. Hashimoto, *Scrip* **2001**, *45*, 455–462.
[20] K. H. Jack, *Acta Crystallogr.* **1952**, *5*, 404–411.
[21] S. Dahl, J. Sehested, C. J. H. Jacobsen, E. Törnvist, I. Chorkendorff, *J. Catal.* **2000**, *192*, 391–399.
[22] C. T. Fishel, R. J. Davis, J. M. Garces, *J. Catal.* **1996**, *163*, 148–157.
[23] R. Pelka, L. Moszynska, W. Arabczyk, *Catal. Lett.* **2009**, *128*, 72–76.
[24] W. Arabczyk, R. Pelka, *J. Phys. Chem. A* **2009**, *113*, 411–415.

Received: June 29, 2010
Published online: November 5, 2010

